https://doi.org/10.1016/j.jcsr.2018.04.030 This is the Pre-Published Version.

Experimental investigation on octagonal concrete filled steel stub columns under uniaxial compression

Jiong-Yi ZHU and Tak-Ming CHAN*

Department of Civil and Environmental Engineering, The Hong Kong Polytechnic University, Hung Hom, Hong Kong

*tak-ming.chan@polyu.edu.hk

Abstract

Concrete filled steel tubes (CFST) have been widely used in modern constructions. The cross-section shapes of circular and rectangular are mostly used. This paper presents an investigation on CFST with a new cross-section shape - octagonal shape which combines both advantages from circular and square cross-sections. In this study, 21 CFST stub columns were tested accompanying with 9 plain concrete columns under uniaxial compression. Three cross-section shapes, octagonal, circular and square sections were considered. In parallel, 10 associated CFST stub columns with octagonal cross-sections from literature were also complied. The measured steel yield strength was between 383 MPa to 485 MPa. Both normal and high strength concrete were used with measured cylinder compressive strengths ranging from 38 MPa to 112 MPa. The key investigation focuses on the relationship between the cross-section shapes and confinement effectiveness which can provide an understanding on the difference in load bearing capacity of CFST with those three section shapes. Design formulae for the cross-section capacity in the current code of practice were assessed by the experimental results and modification was proposed to the existing formula for circular cross-section which could be safely adopted for the CFST with octagonal cross-section.

Keywords: Octagonal concrete filled steel tubes; High strength concrete; Confinement; Cross-section resistance; Design method.

1. Introduction

Concrete filled steel tube (CFST) has shown its superiority in structural efficiency and aesthetics in modern construction. The strength of concrete core could be enhanced by the confinement from steel tube whilst the infilled concrete core could delay the appearance of local buckling of the external steel tube. Investigations have been conducted in the past on the effect of confinement in CFST that indicate the key parameters affecting the performance are cross-section shapes [1-5] and material contribution which is related to the material strengths of both concrete and steel and the diameter to thickness ratio [6-9]. Cross-section shapes of concrete columns have a great impact on the confinement effectiveness when the concrete is under confining pressure from steel stirrups or FRP jacket [10,11]. This phenomenon could also be found in the CFST meanwhile the cross-section shapes may also affect the appearance of the local buckling of steel tubes in those CFST with large diameter to thickness ratio.
The commonly used cross-section shapes in CFST are circular and rectangular sections. With circular cross-section, the steel tube can provide a uniform confining pressure to the concrete core which can efficiently confine the infilled concrete to achieve a good strength enhancement. However, poor confinement effectiveness was found in its counterparts, rectangular CFST. The sharp corners of the rectangular section lead to a stress concentration at corner region while the confinement near the flat side is insufficient [12]. However, the advantage of rectangular CFST is the constructability in the beam-column connection where the flat sides allow the bolted connection with end plate to be assembled. To achieve both the structural efficiency and constructability of CFST, octagonal section is suggested which has a better confinement effectiveness than rectangular section and also could provide flat column sides for construction. A number of investigations have been conducted on CFST with octagonal cross-section shapes. Tomii et al. [13] firstly investigated the axial behaviour of octagonal CFST, it is concluded that the confinement effect of octagonal CFST is somewhere between circular and square CFST. Same conclusion was also found in Susantha et al. [2]. Some experimental investigations were also conducted on the polygonal CFST including octagonal CFST [14,15] and hexagonal CFST [5,15]. Cross-section with elliptical shape was also investigated by many researchers [16-18]. Yu et al. [4] then proposed a unified design method to predict the load capacity of the polygonal CFST. However, existing literature on octagonal CFST is still limited especially on the comparison of other CFST with regular circular and rectangular sections.

This paper extends the existing investigations on octagonal CFST with a comparative experimental investigation on circular, octagonal and square CFST. The results extend the existing database of octagonal CFST with high strength concrete which has a cylinder compressive strength of 112 MPa. The experimental results demonstrate the difference of confinement effect from those three different sections. Modification was applied to the current design formula of load capacity in Eurocode 4 [19] to provide a design solution for load capacity of the octagonal CFST.

2. Experimental investigation

2.1 Specimens

Twenty-one CFST stub columns with cross-section of octagonal, circular and square shapes were prepared. The cross-sectional dimension has been shown in Table 1 where D is the external diameter of the circular section and the external largest width of the octagonal section; b is the width of the flat side of the octagonal and square sections excluding corner region; t is the thickness of steel tubes and L is the length of the specimens (Figure 1). The steel tubes were fabricated by welding two cold-formed half-sections. To study the effect of confinement, identical hollow steel tubes and plain concrete columns which have the same cross-section shape, cross-sectional dimension and material properties were tested independently to capture a superposition value of load capacity from steel tube and concrete core. The companion experiment tests of the hollow steel tubes have been described in Zhu *et al.* [20] and average test results for hollow steel tubes are summarized in Table 2. The plain concrete columns were casted with the CFST using the same batch of concrete. Repeated specimens were made and tested for each configuration of specimens to minimize the effect of the discrete outcome. Specimens with normal strength (measured cylinder strength of 38 MPa) and high strength concrete (measured cylinder strength of 80.5 MPa) have 2 repeated specimens while for those specimens with very high strength concrete (measured cylinder strength of 112.1 MPa), the repeated number is 3. The specimens of CFST were labelled as XY-Z, where X stands for concrete grades; Y stands for cross-section shapes where C is for circular section, O is for octagonal section and S is for square section; Z stands for the number of the repeated specimens, the specimens label start with P are the plain concrete columns without any external steel tube.

2.2 Material

The material properties were collected and based on the tensile coupon tests conducted in Zhu *et al.* [20]. The coupon tests were conducted in accordance with EN ISO 6892-1 [21], for octagonal and square section, coupons were extracted from different locations such as flat side and corner. The material properties from different locations in each hollow section were weighted by their cross-sectional area to obtain an average value for each section. The weighted yield stress of the section is normally larger than that obtained from tensile coupon extracted from flat side which does not consider the strain hardening from the cold forming process. Table 3 shows the material properties from the flat side and the weighted averaged results. $\sigma_{0.2}$, σ_u and E are the 0.2% proof stress, the ultimate stress and the elastic modulus of steel respectively. $\sigma_u/\sigma_{0.2}$ ratio fulfills the requirement in Eurocode 3 [22] (f_u/f_y >1.05). The concrete was commercially sourced and Table 4 shows the mix proportions for each concrete grade. The concrete properties were assessed by the compression tests on standard concrete cylinders and cubes. The dimension of the concrete cylinder was 150 mm diameter × 300 mm height while that of the concrete cube was 150 × 150 × 150 mm. The concrete material tests were conducted within the same week of the main tests on CFST and the test procedure was in accordance with EN 12390-3 [23]. For batches with concrete grades of C25/30 and C50/60, three cylinders and three cubes were tested. Five cylinders and five cubes were tested for the concrete with grades

of C80/95 to avoid high standard deviation due to the brittleness of very high strength concrete. The results of concrete tests were shown in Table 5, where f_{co} and f_{cu} are the cylinder strength and cube strength of concrete respectively, ε_{co} is the axial strain at maximum stress which was measured by the strain gauges with 2% strain limits, E is the elastic modulus of concrete and v is the Poisson ratio. It can be found that the commercial concrete with a certain grade provides a higher cylinder strength which are 38.0, 80.5 and 112.1 MPa for concrete grade of C25/30, C50/60 and C80/95 respectively. These deviations may be caused by a longer curing age (44, 84 and 93 days for C25/30, C50/60 and C80/95 respectively) and a safety margin from the concrete supplier. The strains at maximum stress of C25/30 and C50/60 concrete are 0.0023 and 0.0026 respectively while that in C80/95 concrete is slightly higher (0.003). The elastic modulus was calculated by regression analysis on the region where axial stress ranges from $0.1f_{co}$ to $0.3f_{co}$ which is in accordance with EN 12390-3 [23]. Lateral strain was also measured in the test to capture the Poisson ratio in the mentioned region of the stress-strain curves. Figure 2 shows the stress-axial strain relationship of concrete with different grades. The concrete with measured cylinder strength of 80.5 MPa and 112.1 MPa show a brittle failure within the elastic zone. For normal strength concrete with measured cylinder strength of 38 MPa, the softening behaviour could be observed.

2.3 Stub column tests

Stub column tests were conducted under a compression machine with 1000 tons load capacity. Strain gauges were attached at the middle of the stub columns to capture axial strain and lateral strain of the column under compression. For circular CFST, the strain gauges were attached at the locations 90° apart while in octagonal and square CFST, strains at corner and flat side were recorded. Four LVDTs were mounted around the specimens to record the end-shortening. Figure 3 shows the arrangement of the instrumentations and test set up. Same instrumentations were applied to the plain concrete stub column which has the same section size as the corresponding CFST specimens but without any external steel tube. Steel ring was installed at each end of the CFST specimen to avoid the premature failure at column ends [36]. Figure 4 shows the steel ring at the column end.

2.3.1 Load-end shortening curves and load capacity

There are three types of load-end shortening curves of CFST under axial compression which were illustrated by Han *et al.* [24]. In Figure 5, experimental data collected from current tests show those three types of load-end shortening curves. In all types of load-end shortening responses, a transition zone could be found after the elastic stage because of the yielding of material. Different behaviour shows after the transition zone. Under a high level of confinement, a hardening behaviour was found after the transaction zone. As the level of confinement decreases the hardening stiffness decreases and the post-transition curve becomes a flat line. Below a certain level of the confinement, the softening behaviour occurs with a decreasing softening stiffness. The confinement ratio ξ is used to indicate the level of confinement in Han

et al. [24] to differentiate hardening and softening behaviour of CFST and the boundary value ξ_o is 1.12 and 4.5 for CFST with circular and rectangular cross-section shapes respectively. The definition of confinement ratio ξ is shown as follows:

$$\xi = A_s f_y / A_c f_{co} \quad (1)$$

where A_s and A_c are the cross-sectional area of steel tube and concrete core respectively, f_y is the yield stress of steel tube and f_{co} is the cylinder strength of concrete core. There are a number of definitions of ultimate load and load capacity of CFST in literature. Many researchers agreed that the ultimate load N_u represents the peak load of CFST. It is relatively straight forward to define the peak load in the CFST with a softening post-peak type of behavior. However, in the CFST with a hardening post-peak type of behavior, the peak load cannot be reached even at a very large deformation, therefore some researchers define the peak load when the test ends. Uy *et al.* [25], Tao *et al*. [26] and Wang *et al*. [27] define the ultimate load when the specimens reached an axial strain limitation of 0.01. It is based on the fact that the concrete remains intact and to avoid sudden drop in load due to the crushing of concrete. To demonstrate the use of this definition, the load-end shortening curve of specimen 30C-1, a CFST with strength hardening (ξ =1.54 > boundary value for circular shape) in current test, is shown in Figure 6. It is found that the load at axial strain (defined as the axial shortening/specimen height) of 0.01 is 10.8 % lower than the peak load at axial strain of 0.044. It infers the definition of the ultimate load based on 0.01 axial strain limit [25-27] may be conservative. After machining off the steel tube of the failed specimen, it was observed that the crushing of concrete core only happened in the location where the outward buckling of steel tube occurs while the other part of concrete core keeps its integrity (see Figure 7). Therefore, in this study, it is anticipated that the concrete core can be effectively confined before the inelastic outward buckling of the steel tube occurs in CFST with hardening stress-strain relationship. It is more appropriate to define the ultimate load at the strain when the buckling of the steel tube occurs. In this investigation, it was found that the outward buckling of the steel tube occurred when the load started to drop which means the defined ultimate load is close to the actual peak load of CFST with a hardening post-peak type of behavior.

The test results are shown in Table 6. f_y and f_{co} are the yield strength of steel tube and cylinder strength of concrete core respectively. N_u is the load capacity. The load capacity of repeated specimen shows a very good consistency. Load-end shortening curves for all specimens were plotted Figure 8. To eliminate the effect of different cross-sectional area of the specimens with different cross-section shapes, the normalized axial load N/N_p in y-axis is used where N_p is the plastic resistance of the cross-section of CFST.

$$N_p = A_s f_y + A_c f_{co} \quad (2)$$

In Figure 8, the yield line indicates when the external steel tube starts to yield which is based on the measured yield strain from material tests and the axial strain measured in stub column

tests. The consistency of load-end shortening curves between repeated specimens has been demonstrated in specimens with concrete grades of C25/30 and C50/60, but the softening behaviour cannot be matched for those repeated specimens with concrete grade C80/95 which is due to the brittleness of the concrete core. It can be observed that in Figure 8a, specimens with higher confinement ratio, 30C (ξ=1.54) and 30O (ξ=1.52), show hardening behaviour while the specimens with square cross-section 30S (ξ=1.68) show softening behaviour due to poor confinement effectiveness. For those specimens with higher concrete grades (Figure 8b and 8c), the confinement ratio decreases and only softening behaviour were observed. It should be noted that brittle failure happened at specimens 80S and the softening behaviour cannot be captured because the extremely low confinement effectiveness. In Figure 8, the load-end shortening response of circular and octagonal CFSTs are very close and both better than square CFST in load capacity and ductility. As the concrete grade increases (confinement ratio decreases), the difference in load bearing capacity from various cross-section shapes also decreases. The post-peak portion of the load-shortening curves indicate the ductility of the CFSTs. It could be found the softening slope increases from circular, octagonal and square CFST in sequence in Figure 8a and 8b, which means the ductility of CFST is also related to the confinement effectiveness with each cross-section shape. In Figure 8c, the softening behaviours are not consistent and have no obvious trend due to the low confinement ratio and brittleness of concrete core.

Figure 9 shows the failure mode of some typical specimens and the failure mode of concrete core after removal of the external steel tube. It could be found that the local buckling of steel tube happens at where the concrete crushed. The damage of high strength concrete is more serious than that with normal strength concrete which could explain the softening behaviour and rapid load drop in those specimens with high strength concrete.

2.3.2 Confinement

In CFST, the load capacity is enhanced by the interaction of steel tubes and concrete core comparing with the plastic resistance of the composite section which is the added compression resistance of steel and concrete components. However, the plastic resistance may not be equal to the actual compression resistance of the individual steel and concrete components because it does not consider the strain hardening in hollow steel tube and concrete strength reduction in high strength concrete due to the brittleness. In order to capture the actual compressive resistance from each individual component in the CFSTs, hollow steel tube (Table 2) and plain concrete column with the same geometric properties were tested and compared with the load capacity of CFST to investigate the confinement effectiveness from each cross-section shape. Table 7 shows the test results of plain concrete column where $f_{co,c}$ is the compressive strength of plain concrete column. It was found that the concrete strengths of plain concrete columns are smaller than the strengths obtained from standard cylinder tests especially for the concrete with cylinder strength larger than 80 MPa and the reduction ratio is about 0.9. This observation could be explained by a smaller axial strain at failure found in the column with a larger scale.

It is indicated that under the same elastic modulus, the columns with larger scale have a premature failure comparing with that in the standard cylinder specimens. The possible reason for the premature failure in the large-scale column is that the non-uniform distribution of concrete properties along the column height has a greater impact to the brittleness of high strength concrete; this non-uniform property distribution is caused by the vertical casting of concrete in a column leading to sedimentation and water gain in the top region of a column [28]. In Eurocode 2 [29], effective compressive strength was adopted for those concrete with cylinder strength within 50 MPa to 90 MPa and Liew and Xiong [30] extended the effective strength to those ultra-high strength concrete with cylinder strength larger than 90 MPa. The effective strength coefficient proposed by Liew and Xiong [30] is shown as follows:

$$\eta = \begin{cases} 1.0 - (f_{co} - 50)/200 & 50\text{MPa} < f_{co} \le 90\text{MPa} \\ 0.8 & f_{co} > 90\text{MPa} \end{cases} \quad (3)$$

Figure 10 shows a comparison of load-end shortening curves of CFST and a simple superposition model of steel tubes and plain concrete column (Specimen 30O-1). It could be found that the plain concrete fails with a small axial strain while in CFST the steel tube prevents the failure of concrete core and significantly increase the ductility of the column. The load capacity from CFST is larger than the sum of load capacity from individual components which could be indicated by the gaps in Figure 10 due to the benefit from the effect of confinement.

The difference in confinement effectiveness caused by cross-section shape significantly affects the performance of axial load capacity in CFST. In octagonal CFST, part of concrete core near the flat region of steel tube cannot be effectively confined and this loss of confinement effect will reduce the load capacity comparing with its circular counterparts. The non-uniform confinement in octagonal and square CFST could be explained by the measured hoop strain in the tests. Figure 11 shows the normalized axial load to hoop strain relationship of specimens with different concrete grade. It could be found although the hoop strain at column side of octagonal CFST is similar to that in circular CFST but the hoop strain at corner is much lower. The interpretation is that insufficient confinement at flat side allows the concrete expanding more than that in corner region. This phenomenon could be found in CFSTs with all three different concrete grades. Thus, it is crucial to identify the loss in load capacity due to decline of the confinement effectiveness. Table 8 shows the enhanced percentage in load capacity of CFST comparing with the simple superposition model of two individual components where N_s is the superposition model with a sum of load capacity of steel tube and plain concrete core.

$$N_s = N_{steel} + N_{concrete} \quad (4)$$

where N_{steel} is the compressive resistance of the hollow steel tube (Table 2) and $N_{concrete}$ is the load capacity of concrete core which is calculated from the core area times the averaged strength of the plain concrete columns. The results show the enhanced percentages are significant in the circular and octagonal CFST under high confinement ratio (ξ=1.54) which

can be up to 32.1%. It is obvious that the load capacity enhancement ratio is related to the confinement ratio ξ. It should be noted that as the confinement ratio decreases the difference between the load-capacity enchantment ratio of circular and octagonal CFST becomes negligible. The difference between N_s and N_p is because the strain hardening of steel tube and strength reduction on high strength concrete are not considered in plastic resistance. The results show the as anticipated enhancement in square CFST could be neglected due to the poor confinement effectiveness.

Based on the observation in the confinement effect of circular and octagonal CFST, it is concluded that under similar confinement ratio, the enhancement in load capacity of octagonal CFST is smaller than that in circular CFST but only up to 8%, however the enhancement is much better than the square CFST with 16% in maximum.

3. Design of octagonal CFST

3.1 Existing code of practice

The existing design codes provide design formulae for the load capacity of CFST stub columns. Most of the design codes only cover CFST with circular and rectangular sections. To promote the application of octagonal CFST, the assessment on current design formulae should be conducted to understand the existing limitation on design of octagonal CFST. It should be noted the averaged compressive strength of plain concrete column and the yield stress of steel from the flat coupons in octagonal and square section and curved coupon in circular section were used in the design assessment for those test data presented in this paper.

3.1.1 Eurocode 4 [19]/AS 5100 [31]

In Eurocode 4 [19], based on plastic analysis, two formulae are suggested, one for those CFST with general cross-section shapes and another one especially for circular CFSTs which considers the confinement effect. The formulae are shown as follows:

$$N_d = A_s f_y + A_c f_{co} \qquad \text{for gerneral sections} \tag{5}$$

$$N_d = \eta_a A_s f_y + A_c f_{co}\left(1+\eta_c \frac{t}{d}\frac{f_y}{f_{co}}\right) \qquad \text{for circular section} \tag{6}$$

In the case of uniaxial load:

$$\eta_a = 0.25\left(3+2\bar{\lambda}\right) \le 1$$
$$\eta_c = 4.9 - 18.5\bar{\lambda} + 17\bar{\lambda}^2 \ge 0 \tag{7}$$

where N_d is the design value of load capacity, η_a and η_c is the modification factor on steel tube

and concrete core related to confinement of concrete, t is the thickness of steel tube and d is the outer diameter of circular CFST. Eurocode 4 also gives the limitation on steel yield strength, concrete strength and maximum D/t ratio for the application of the formulae:

$D/t \leq 90(235/f_y)$ circular (8)
$B/t \leq 52\sqrt{(235/f_y)}$ rectangular (9)
$235 \text{ MPa} \leq f_y \leq 460 \text{ MPa}$ (10)
$20 \text{ MPa} \leq f_{co} \leq 50 \text{ MPa}$ (11)

The suggested design formulae in Australian design code AS 5100 [31] are basically the same as those in Eurocode 4, but with different limitations:

$D/t \leq 82(250/f_y)$ circular (12)
$B/t \leq 35\sqrt{(250/f_y)}$ rectangular (13)
$230 \text{ MPa} \leq f_y \leq 400 \text{ MPa}$ (14)
$25\text{MPa} \leq f_{co} \leq 65 \text{ MPa}$ (15)

3.1.2 American code [32,33]

ACI 318-11 [32] suggests a very simple formula for the design of load capacity. A sum of load capacity of each components is shown as follows:

$$N_d = A_s f_y + 0.85 A_c f_{co} \quad (16)$$

AISC 360-16 [33] further indicated the confinement effect should be considered in the circular CFST and suggested using $0.95f_{co}$ instead of $0.85f_{co}$. The formula for circular section is shown as:

$N_d = A_s f_y + 0.95 A_c f_{co}$ for circular section (17)

AISC 360-16 also gives the limitation on D/t ratio, yield strength of steel and concrete strength:
$D/t \leq 0.15E/f_y$ circular (18)
$B/t \leq 2.26\sqrt{(E/f_y)}$ rectangular (19)
$f_y \leq 525MPa$ (20)
$21MPa \leq f_{co} \leq 70MPa$ (21)

3.2 Assessment of current code

The test data of circular and square CFST specimens in current experimental investigation were first being used to assess the applicability of the design codes. Table 9 demonstrates the result of the assessment where a better prediction from Eurocode 4 was found on both the load capacity of circular and square CFST. Although the plain concrete strength of those specimens (60C, 60S, 80C, 80S) are larger than the suggested limitation (60 MPa) in Eurocode 4, the code

still can capture the test results very well. The maximum deviation is only about 2.9% in circular CFST. For those square CFST, both design codes can give a reasonable prediction on the test data within their limitations but less accurate in the specimens with high strength concrete. The maximum deviation is up to 3.2%. The American specifications [32,33] provide a conservative prediction.

The existing codes of practice have shown their applicability on circular and square CFSTs. Further assessment was conducted to check if the formulae for general cross-section shape is suitable for octagonal CFSTs. In addition to current experimental data of octagonal CFSTs, test results of 10 more octagonal CFSTs from Ding et al. [14] and Zhu and Chan [15] were also used in this assessment. Although the experimental works of Tomii *et al.* [13] are recognized, the test results are not included in current database due to a high level of deviations [4,34] and the limited access of the original dataset. The current database of octagonal CFST is summarized in Table 10. It should be noted that the cylinder strength from Zhu and Chan [15] is larger than 90 MPa and the effective coefficient 0.8 from Eq. 3 was applied in the assessment. The assessment results are shown in Table 11. The design formula for general cross-section which does not consider the confinement effect underestimates the load capacity of the octagonal specimens with 16.5% in Eurocode 4 and AS 5100 while the formula in American specification is more conservative (See Table 11).

3.3 Proposed design method

The assessment shows that the confinement effect on load capacity of octagonal CFST cannot be neglected and current design code for general cross-section shapes is not applicable. However, Eurocode 4 shows a very accurate prediction on the circular CFST, thus, it is possible to find an equivalent circular section of the octagonal section to make the design formula applicable to the octagonal CFST. The design formula for load capacity could be developed by a basic superposition model with modification factors which is shown as follows:

$$N_d = \alpha_s A_s f_y + \left(1+\alpha_c\right) A_c f_{co} \tag{22}$$

where α_s is the reduction factor on steel tube as the axial stress of steel tube cannot reach the yield stress due to the biaxial stress condition. α_c is the enhancement factor to concrete core because the effect of confinement. The steel tube in CFST is under the axial stress σ_a from the applied load and hoop stress σ_h from the dilation of concrete after the elastic stage. As the stress in concrete approaching its unconfined strength, the hoop strain increases rapidly and larger than that in steel tubes and then the steel tube starts to confine the concrete and the steel tube is under biaxial stress condition. To determine the reduction factor α_s, the hoop stress in steel tubes is critical. In existing literature and design codes [19,27], the reduction factor α_s in circular CFST have been well established. Thus, it is possible to obtain the reduction factor α_s in octagonal CFST by investigating the relationship between the hoop stress in the CFST with circular and octagonal section. Liu *et al.* [35] established a simple cross-section equilibrium as

shown in Figure 12. Based on this equilibrium the hoop stress of octagonal could be derived as:

$$\sigma_{h,s} = \frac{f_l \left(D_i - t \right)}{2t} \tag{23}$$

where $\sigma_{h,s}$ is the hoop stress of the steel tube, f_l is the confining pressure and D_i is the inscribed diameter of the octagonal section.

$$D_i = \left(1 + \sqrt{2} \right) B \tag{24}$$

where B is the nominal width of the octagonal section including the corner radius. It was found that the hoop stress in steel tube of octagonal CFST is equal to that in CFST with the inscribed circular section. Based on this finding, the equivalent circular section with an inscribed diameter of D_i could be used to determine the reduction factor α_s where

$$\alpha_{s,\,oct} = \alpha_{s,\,Di} \tag{25}$$

It is believed that under the same confinement ratio or material contribution ratio, the enhancement factor is only affected by the cross-sectional shapes of CFST and it is found that with the same tube thickness the inscribed circular section shares the same confinement ratio with the original octagonal section. According to this assumption, it is possible to find a relationship between the enhancement factor α_c of octagonal section and that of its inscribed circular section which satisfy

$$\alpha_{c,\,oct} = k\alpha_{c,\,Di} \tag{26}$$

where $\alpha_{c,\,Di}$ and $\alpha_{c,\,oct}$ are the enhancement factor of the inscribed circular section and the octagonal section respectively. k is the shape factor that reflect the confinement effectiveness. Previous assessment (see Table 8) has shown the difference in the enhancement percentage of the load capacity between circular and octagonal CFST. As the circular and octagonal specimens in this experimental investigation share a similar confinement ratio, which means that the difference of enhancement percentage in Table 8 is only caused by the change of cross-section shapes. Thus the enhancement difference in Table 8 could be used to investigate the relationship between $\alpha_{c,Di}$ and $\alpha_{c,oct}$. Figure 13 shows the relationship between the load capacity enhancement percentage in circular CFST $\alpha_{c,Di}$ and that in octagonal CFST, $\alpha_{c,oct}$. It could be found the relationship is approximately linear and the k value is about 0.73. This observation is consistent with that the concept of effective confined area which is firstly proposed by Mander *et al.* [10] for the spirals confined concrete and then widely used in the non-uniformly confined concrete with cross-section such as rectangular and polygonal sections [4,12,14]. It is concluded that the effective confined area are nearly 70 percent of the total area of octagonal cross-section [4,14].

Based on Eq. (25) and Eq. (26), the design formula for circular CFST in Eurocode 4, Eq. (6) could be modified for the design of octagonal CFST as follows:

$$N_d = \eta_{a,Di} A_s f_y + A_c f_{co} \left(1 + 0.73 \eta_{c,Di} \frac{t}{D_i} \frac{f_y}{f_{co}} \right) \tag{27}$$

where $\eta_{a,Di}$ and $\eta_{c,Di}$ are the modification factor which is calculated from Eq. (7) based on the equivalent inscribed circular section.

Figure 14 shows the assessment of the proposed design formula for octagonal CFST. It could be found that the modified design formula can provide a very close and conservative prediction on the load capacity of octagonal CFST comparing with existing design methods. All the predictions fall into the safe zone in Figure 13. Table 12 also shows the satisfactory performance of the proposed method. This proposed method could apply to octagonal CFST with concrete cylinder strength ranging from 32 to 112 MPa with normal strength steel tube with yield strength from 296 to 383 MPa.

4. Conclusions

This paper presented an experimental investigation on the octagonal CFST. Accompanying circular and square CFST specimens were also tested. The test results show that under a high confinement ratio, the confinement effectiveness of octagonal CFST in terms of enhancement in axial resistance is not comparable to that in circular CFST, but is much better than that in square CFST. However, when the high strength concrete was used where the confinement ratio decreased, the difference in the enhancement in load capacity between circular and octagonal CFST becomes negligible. The current design formula in Eurocode 4 [19], Australian code [31] and American code [32,33] underestimate the load capacity of octagonal CFST because the effect of confinement is not considered. Based on the design formula in Eurocode 4 for circular CFST, equivalent circular section approach was proposed which modifies the current design equation applicable for octagonal CFST. The proposed design method on octagonal CFST shows a good prediction on the existing experimental results.

Acknowledgement

Authors are thankful to WoLee steel Co. Ltd. for supplying the test specimens. This paper was also partly supported by the research funding from the Construction Industry Council under the project “Application of Polygonal High Strength Concrete-filled Composite Column in Seismic-resistant Buildings in Hong Kong”. The support from the Chinese National Engineering Research Centre for Steel Construction (Hong Kong Branch) is also gratefully acknowledged.

References

[1] Schneider, S.P., 1998. Axially loaded concrete-filled steel tubes. *Journal of structural Engineering*, *124*(10), pp.1125-1138.

[2] Susantha, K.A.S., Ge, H. and Usami, T., 2001. Uniaxial stress–strain relationship of concrete confined by various shaped steel tubes. *Engineering Structures*, *23*(10), pp.1331-1347.

[3] Han, L.H., 2002. Tests on stub columns of concrete-filled RHS sections. *Journal of Constructional Steel Research*, *58*(3), pp.353-372.

[4] Yu, M., Zha, X., Ye, J. and Li, Y., 2013. A unified formulation for circle and polygon concrete-filled steel tube columns under axial compression. *Engineering structures*, *49*, pp.1-10.

[5] Xu, W., Han, L.H. and Li, W., 2016. Performance of hexagonal CFST members under axial compression and bending. *Journal of Constructional Steel Research*, *123*, pp.162-175.

[6] Gardner, N.J. and Jacobson, E.R., 1967. Structural behavior of concrete filled steel tubes. *Journal Proceedings 64*(7), pp. 404-413.

[7] Giakoumelis, G. and Lam, D., 2004. Axial capacity of circular concrete-filled tube columns. *Journal of Constructional Steel Research*, *60*(7), pp.1049-1068.

[8] Ellobody, E., Young, B. and Lam, D., 2006. Behaviour of normal and high strength concrete-filled compact steel tube circular stub columns. *Journal of Constructional Steel Research*, *62*(7), pp.706-715.

[9] Liew, J.R., Xiong, M.X. and Xiong, D.X., 2014. Design of High Strength Concrete Filled Tubular Columns for Tall. *Int. J. High-Rise Build*, *3*.

[10] Mander, J.B., Priestley, M.J. and Park, R., 1988. Theoretical stress-strain model for confined concrete. *Journal of structural engineering*, *114*(8), pp.1804-1826.

[11] Teng, J., Huang, Y.L., Lam, L. and Ye, L.P., 2007. Theoretical model for fiber-reinforced polymer-confined concrete. *Journal of composites for construction*, *11*(2), pp.201-210.

[12] Lam, L. and Teng, J.G., 2003. Design-oriented stress-strain model for FRP-confined concrete in rectangular columns. *Journal of Reinforced Plastics and Composites*, *22*(13), pp.1149-1186.

[13] Tomii, M., Kosi Y., and Yoichi M., 1977. "Experimental studies on concrete-filled steel tubular stub columns under concentric loading." In Stability of Structures Under Static and Dynamic Loads, pp. 718-741. ASCE.

[14] Ding, F.X., Li, Z., Cheng, S. and Yu, Z.W., 2016. Composite action of octagonal concrete-filled steel tubular stub columns under axial loading. Thin-Walled Structures, 107, pp.453-461.

[15] Zhu, J.Y. and Chan, T.M., 2018. Behaviour of polygonal-shaped steel-tube columns filled with high-strength concrete. *Proceedings of the Institution of Civil Engineers-Structures and Buildings*, 171(2),96-112.

[16] Sheehan, T., Dai, X.H., Chan, T.M. and Lam, D., 2012. Structural response of concrete-filled elliptical steel hollow sections under eccentric compression. Engineering Structures, 45, pp.314-323.

[17] Chan, T.M., Huai, Y.M. and Wang, W., 2015. Experimental investigation on lightweight concrete-filled cold-formed elliptical hollow section stub columns. Journal of Constructional Steel Research, 115, pp.434-444.

[18] Liu, F., Wang, Y. and Chan, T.M., 2017. Behaviour of concrete-filled cold-formed elliptical hollow

sections with varying aspect ratios. Thin-Walled Structures, 110, pp.47-61.

[19] EN 1994-1-1, 2004. Eurocode 4 Design of steel and concrete structures, Part 1.1, General rules and rules for buildings. Brussels: European Committee for Standardization CEN.

[20] Zhu, J.Y., Chan, T.M. and Young, B., 2017. Structural behaviour of octagonal tubular steel stub columns under uniaxial compression. In*: Proceedings of the 16th International Symposium for Tubular Structures,* pp.567-573. Melbourne.

[21] European Committee for Standardization, 2009. BS EN ISO 6892-1:2009. Metallic materials - Tensile testing. Part 1: Method of test at ambient temperature. Brussels.

[22] EN 1993-1-1, 2005. Eurocode 3: Design of steel structures – Part 1.1: General rules and rules for buildings. Brussels: European Committee for Standardization CEN.

[23] EN 12390-3, 2009. Testing hardened concrete: Compressive strength of test specimens. Brussels: European Committee for Standardization CEN.

[24] Han, L.H., Yao, G.H. and Zhao, X.L., 2005. Tests and calculations for hollow structural steel (HSS) stub columns filled with self-consolidating concrete (SCC). *Journal of Constructional Steel Research*, *61*(9), pp.1241-1269.

[25] Uy, B., Tao, Z. and Han, L.H., 2011. Behaviour of short and slender concrete-filled stainless steel tubular columns. *Journal of Constructional Steel Research*, *67*(3), pp.360-378.

[26] Tao, Z., Wang, Z.B. and Yu, Q., 2013. Finite element modelling of concrete-filled steel stub columns under axial compression. *Journal of Constructional Steel Research*, *89*, pp.121-131.

[27] Wang, Z.B., Tao, Z., Han, L.H., Uy, B., Lam, D. and Kang, W.H., 2017. Strength, stiffness and ductility of concrete-filled steel columns under axial compression. *Engineering Structures*, *135*, pp.209-221.

[28] Park, R. and Paulay, T., 1975. *Reinforced Concrete Structures.* John Wiley & Sons, New York.

[29] EN 1992-1-1,2004. Eurocode 2: Design of concrete structures, Part 1.1, General rules and rules for buildings. Brussels: European Committee for Standardization CEN.

[30] Liew, J.R. and Xiong, M., 2015. *Design guide for concrete filled tubular members with high strength materials to Eurocode 4*. Research Publishing.

[31]AS5100, 2004. Australia Standard. Bridge design, Part 6: steel and composite construction, Sydney, Australia.

[32] ACI 318-11, 2011. Building code requirements for structural concrete and commentary. American Concrete Institute (ACI), Farmington Hills, MI.

[33] AISC 360-16, 2016. Specification for structural steel buildings, American Institute of Steel Construction (AISC), Chicago (IL).

[34] Hassanein, M.F., Patel, V.I., Elchalakani, M. and Thai, H.T., 2018. Finite element analysis of large diameter high strength octagonal CFST short columns. *Thin-Walled Structures*, *123*, pp.467-482.

[35] Liu, S.W., Chan, T.M., Chan, S.L. and So, D.K.L., 2017. Direct analysis of high-strength concrete-filled-tubular columns with circular & octagonal sections. *Journal of Constructional Steel Research*, *129*, pp.301-314.

[36] Ma JL, Chan TM, Young B. Experimental investigation on stub-column behavior of cold-formed high-strength steel tubular sections. J Struct Eng 2016; 142(5): 04015174.

Table 1

Cross-sectional dimension of the specimens.

Cross-section	D (mm)	B (mm)	b (mm)	t (mm)	L (mm)	D/t or b/t
Octagonal	178	73.7	60	5.6	695	31.8 or 10.7
Circular	200	-	-	6.0	695	33.3
Square	-	200	179	6.0	695	29.8

Table 2

Experimental data of hollow steel tubes.

Stub column	N_u (kN)	$\sigma_{0.2,sc}$ (MPa)	$\sigma_{u,sc}$ (MPa)
OctHS	1452	400	468
CHS	1787	484	502
SHS	2186	---	470

Table 3

Material properties of steel.

Cross-section	$\sigma_{0.2}$ (MPa)	σ_u (MPa)	E (GPa)	$\sigma_u/\sigma_{0.2}$
Octagonal-*flat*	383	504	212	1.32
Octagonal-*avg*	413	521	214	1.26
Circular	451	577	215	1.28
Square-*flat*	477	571	219	1.20
Square-*avg*	485	584	217	1.20

Table 4

Mix proportions of concrete per m^3.

	Cement (kg)	Fly ash (kg)	Silica Fume (kg)	Water (kg)	Coarse Aggregate (5-10 mm) (kg)	Coarse Aggregate (10-20 mm) (kg)	Fine Aggregate (kg)	Superplasticizer (kg)	Polypropylene Fibre (kg)	Water/cement ratio
C25/30	400	0	0	220	840	0	810	3.78	0	0.55
C50/60	412	138	0	180	235	570	800	7.58	0	0.33
C80/95	360	190	33	156	795	0	765	13.4	2	0.27

Table 5

Concrete properties.

Concrete	f_{co} (MPa)	f_{cu} (MPa)	ε_{co}	E (GPa)	v
C25/30	37.7	46.8	0.0024	27600	0.19
	38.2	47.2	0.0021	28000	0.19
	38.2	47.0	0.0025	27300	0.20
Mean	*38.0*	*47.0*	*0.0023*	*27600*	*0.19*
C50/60	80.0	92.5	0.0027	35200	0.21
	80.9	95.2	0.0026	34900	0.20
	80.6	93.3	0.0027	35100	0.20
Mean	*80.5*	*93.7*	*0.0026*	*35100*	*0.20*
C80/95	111.9	120.8	0.0029	40400	0.21
	110.2	123.3	0.0029	40000	0.19
	113.9	119.6	0.0031	39700	0.20
	111.0	118.5	0.0030	41000	0.20
	113.5	123.5	0.0030	40900	0.19
Mean	*112.1*	*121.1*	*0.0030*	*40400*	*0.20*

Table 6

Results of stub column tests.

Specimens	f_y (MPa)	f_{co} (MPa)	ξ	$> \xi_o$	N_u (kN)
30C-1	451	38	1.54	Y	3503
30C-2	451	38	1.54	Y	3519
30O-1	413	38	1.52	*NA*	2733
30O-2	413	38	1.52	*NA*	2680
30S-1	485	38	1.68	N	3488
30S-2	485	38	1.68	N	3452
50C-1	453	80.5	0.73	N	4463
50C-2	453	80.5	0.73	N	4423
50O-1	413	80.5	0.71	*NA*	3543
50O-2	413	80.5	0.71	*NA*	3549
50S-1	485	80.5	0.79	N	4921
50S-2	485	80.5	0.79	N	4973
80C-1	453	112.1	0.53	N	5071
80C-2	453	112.1	0.53	N	5040
80C-3	453	112.1	0.53	N	5099
80O-1	413	112.1	0.51	*NA*	4199
80O-2	413	112.1	0.51	*NA*	4153
80O-3	413	112.1	0.51	*NA*	4203
80S-1	485	112.1	0.57	N	6060
80S-2	485	112.1	0.57	N	6298
80S-3	485	112.1	0.57	N	6218

Table 7

Test results of plain concrete columns.

Specimen	Cross-section	$f_{co,c}$	f_{co} (from Table 5)	$f_{co,c}/f_{co}$
P30C	Circular	37.1	38	0.98
P30O	Octagonal	38.2	38	1.01
P30S	Square	39.3	38	1.03
Mean		*38.2*		*1.01*
P50C	Circular	71.4	80.5	0.89
P50O	Octagonal	73.7	80.5	0.92
P50S	Square	72.1	80.5	0.90
Mean		*72.4*		*0.90*
P80C	Circular	100.5	112.1	0.90
P80O	Octagonal	100.1	112.1	0.89
P80S	Square	100.1	112.1	0.89
Mean		*100.2*		*0.89*

Table 8

Enhancement ratio in load capacity.

Specimen	ξ	N_u (kN)	N_s (kN)	N_p (kN)	N_u/N_s	N_u/N_p
30C-1	1.54	3503	2832	2659	1.237	1.318
30C-2	1.54	3519	2832	2659	1.243	1.324
		Mean δ			*24.0%*	*32.1%*
30O-1	1.52	2733	2329	2202	1.173	1.241
30O-2	1.52	2680	2329	2202	1.151	1.217
		Mean δ			*16.2%*	*22.9%*
30S-1	1.68	3488	3529	3601	0.989	0.969
30S-2	1.68	3452	3529	3601	0.978	0.959
		Mean δ			*-1.7%*	*-3.6%*
50C-1	0.73	4463	3778	3835	1.181	1.164
50C-2	0.73	4423	3778	3835	1.171	1.153
		Mean δ			*17.6%*	*15.9%*
50O-1	0.71	3543	3141	3205	1.128	1.106
50O-2	0.71	3549	3141	3205	1.130	1.107
		Mean δ			*12.9%*	*10.7%*
50S-1	0.79	4921	4744	5103	1.037	0.964
50S-2	0.79	4973	4744	5103	1.048	0.975
		Mean δ			*4.3%*	*-3.1%*
80C-1	0.53	5071	4543	4704	1.116	1.078
80C-2	0.53	5040	4543	4704	1.109	1.071
80C-3	0.53	5099	4543	4704	1.122	1.084
		Mean δ			*11.6%*	*7.8%*
80O-1	0.51	4199	3789	3942	1.108	1.065
80O-2	0.51	4153	3789	3942	1.096	1.054
80O-3	0.51	4203	3789	3942	1.109	1.066
		Mean δ			*10.4%*	*6.2%*
80S-1	0.57	6060	5727	6220	1.058	0.974
80S-2	0.57	6298	5727	6220	1.100	1.013
80S-3	0.57	6218	5727	6220	1.086	1.000
		Mean δ			*8.1%*	*-0.5%*

Table 9

Design assessment in circular and square CFST.

	Eurocode 4/AS 5100		ACI/AISC	
	N_d (kN)	N_d/N_u	N_d (kN)	N_d/N_u
Circular CFST				
30C-1	3637	1.038	2614	0.714
30C-2	3637	1.033	2614	0.711
50C-1	4518	1.012	3513	0.741
50C-2	4518	1.021	3513	0.748
80C-1	5235	1.032	4237	0.780
80C-2	5235	1.039	4237	0.785
80C-3	5235	1.027	4237	0.775
Mean		*1.029*		*0.750*
Square CFST				
30S-1	3564	1.022	3363	0.964
30S-2	3564	1.033	3363	0.974
50S-1	4780	0.971	4396	0.893
50S-2	4780	0.961	4396	0.884
80S-1	5759	0.950	5228	0.863
80S-2	5759	0.914	5228	0.830
80S-2	5759	0.926	5228	0.841
Mean		*0.968*		*0.893*

Table 10

Database of octagonal CFST stub columns.

	f_y (MPa)	$f_{co,c}$ (MPa)	b (mm)	t (mm)	N_u (kN)
Current experimental investigation					
30O1-1	383	38.0	60	5.6	2733
30O1-2	383	38.0	60	5.6	2680
50O1-1	383	72.4	60	5.6	3543
50O1-2	383	72.4	60	5.6	3549
80O1-1	383	100.2	60	5.6	4199
80O1-2	383	100.2	60	5.6	4153
80O1-3	383	100.2	60	5.6	4203
Zhu and Chan (2018)					
O-CF-1	296	80.2	59.5	2.9	1970
O-CF-2	296	80.2	59.5	2.9	2024
Ding et al. (2016)					
OST1-A	311	32	201	3.85	9297
OST1-B	311	32	199	3.98	9311
OST2-A	321	32	200	6.02	10502
OST2-B	321	32	197	5.89	10713
OST3-A	311	46	200	3.92	12362
OST3-B	311	46	199	4.02	12357
OST4-A	321	46	197	5.88	12992
OST4-B	321	46	198	5.98	13263

Table 11

Assessment for octagonal CFST with current codes.

	Eurocode 4/AS 5100		ACI/AISC	
	N_d (kN)	N_d/N_u	N_d (kN)	N_d/N_u
Current experimental investigation				
30O-1	2118	0.775	1988	0.726
30O-2	2118	0.790	1988	0.741
50O-1	2920	0.824	2670	0.753
50O-2	2920	0.823	2670	0.751
80O-1	3584	0.854	3235	0.770
80O-2	3584	0.863	3235	0.778
80O-3	3584	0.853	3235	0.769
Mean		*0.826*		*0.755*
Zhu and Chan (2018)				
O-CF-1	1666	0.846	1476	0.814
O-CF-2	1666	0.823	1476	0.792
Mean		*0.834*		*0.803*
Ding et al. (2016)				
OST1-A	7955	0.856	7049	0.758
OST1-B	7871	0.845	6984	0.750
OST2-A	8929	0.850	8047	0.766
OST2-B	8645	0.807	7790	0.727
OST3-A	10532	0.852	9243	0.748
OST3-B	10474	0.848	9201	0.745
OST4-A	11136	0.857	9906	0.762
OST4-B	11279	0.850	10038	0.757
Mean		*0.846*		*0.752*
Overall Mean		*0.835*		*0.753*

Table 12

Assessment of octagonal CFST with proposed design method

	Proposed design method	
	N_d (kN)	N_d/N_u
Current experimental investigation		
30O-1	2598	0.951
30O-2	2598	0.969
50O-1	3366	0.950
50O-2	3366	0.948
80O-1	3993	0.951
80O-2	3993	0.962
80O-3	3993	0.950
Mean		*0.954*
Zhu and Chan (2018)		
O-CF-1	1833	0.930
O-CF-2	1833	0.906
Mean		*0.918*
Ding et al. (2016)		
OST1-A	8829	0.950
OST1-B	8763	0.941
OST2-A	10323	0.983
OST2-B	9984	0.932
OST3-A	11393	0.922
OST3-B	11354	0.919
OST4-A	12440	0.958
OST4-B	12614	0.951
Mean		*0.944*
Overall Mean		*0.939*

Table 14

Summary of parameters in reliability analysis.

Data set	No. of specimens	$k_{d,n}$	b	V_δ	γ_m
Current test	7	5.60	1.02	0.042	1.02
Current test + existing literature	17	3.75	1.06	0.014	0.98

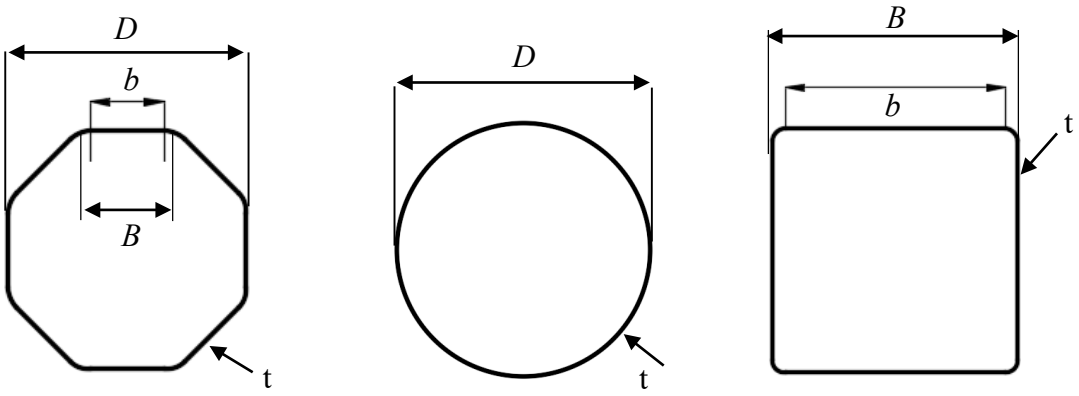

Octagonal - OctHS Circular - CHS Square - SHS

Figure 1. Dimension of specimens

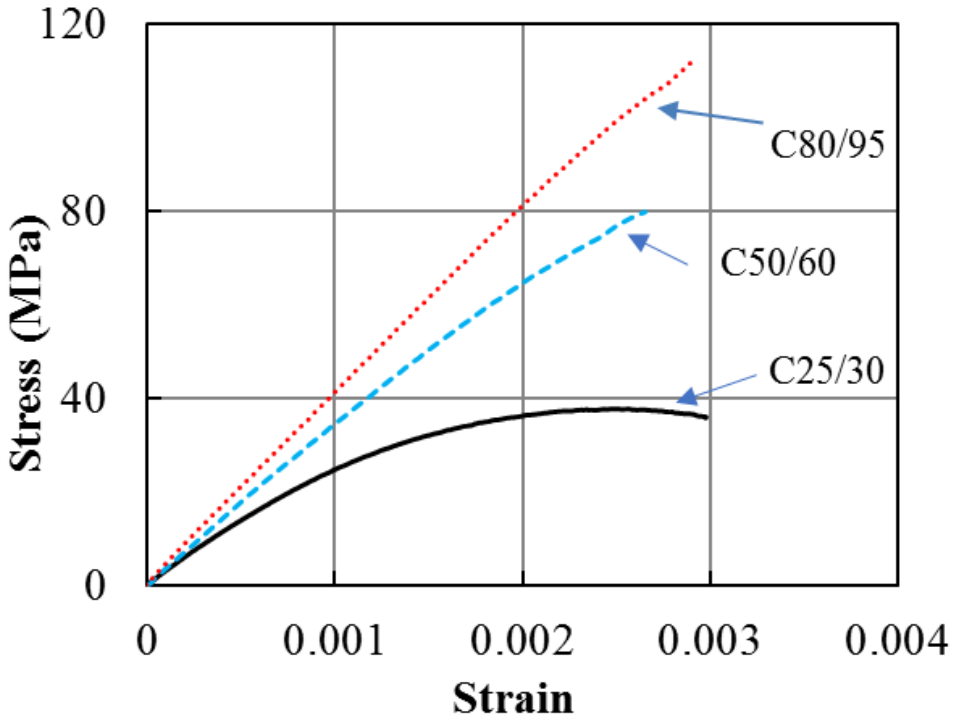

Figure 2. Stress- axial strain relationship

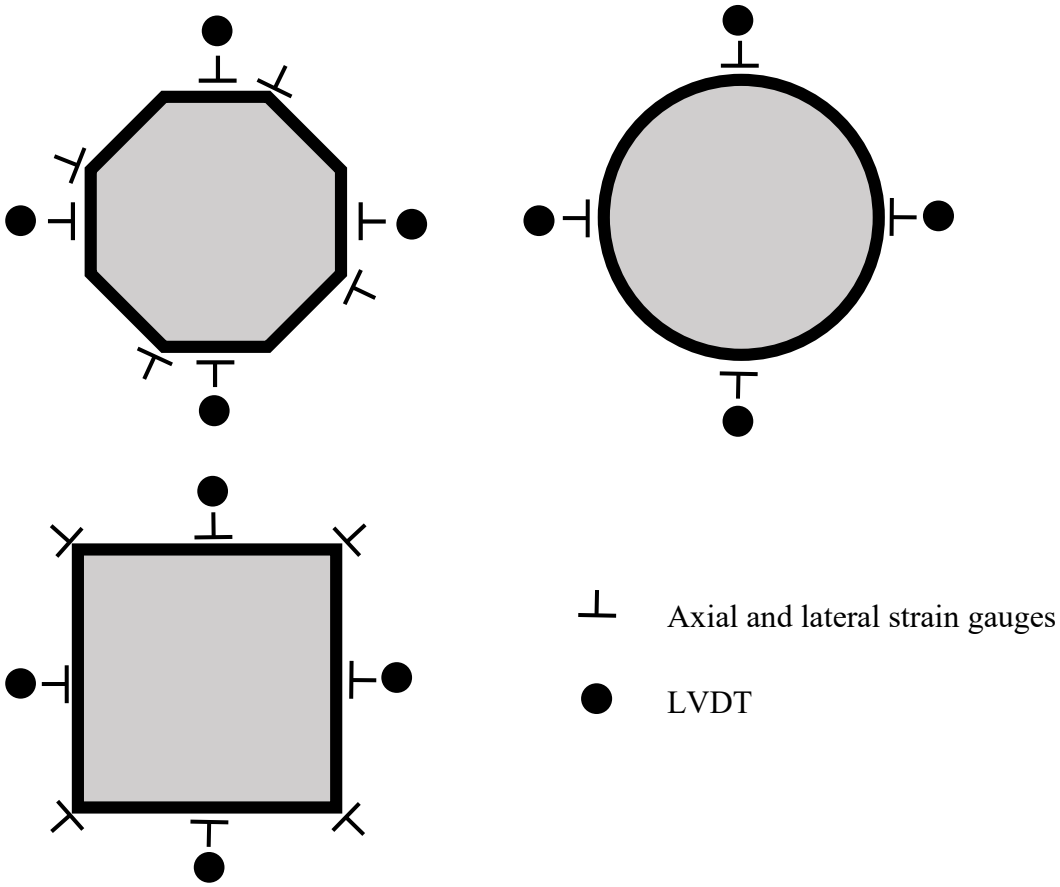

(a) Arrangement of the instrumentations

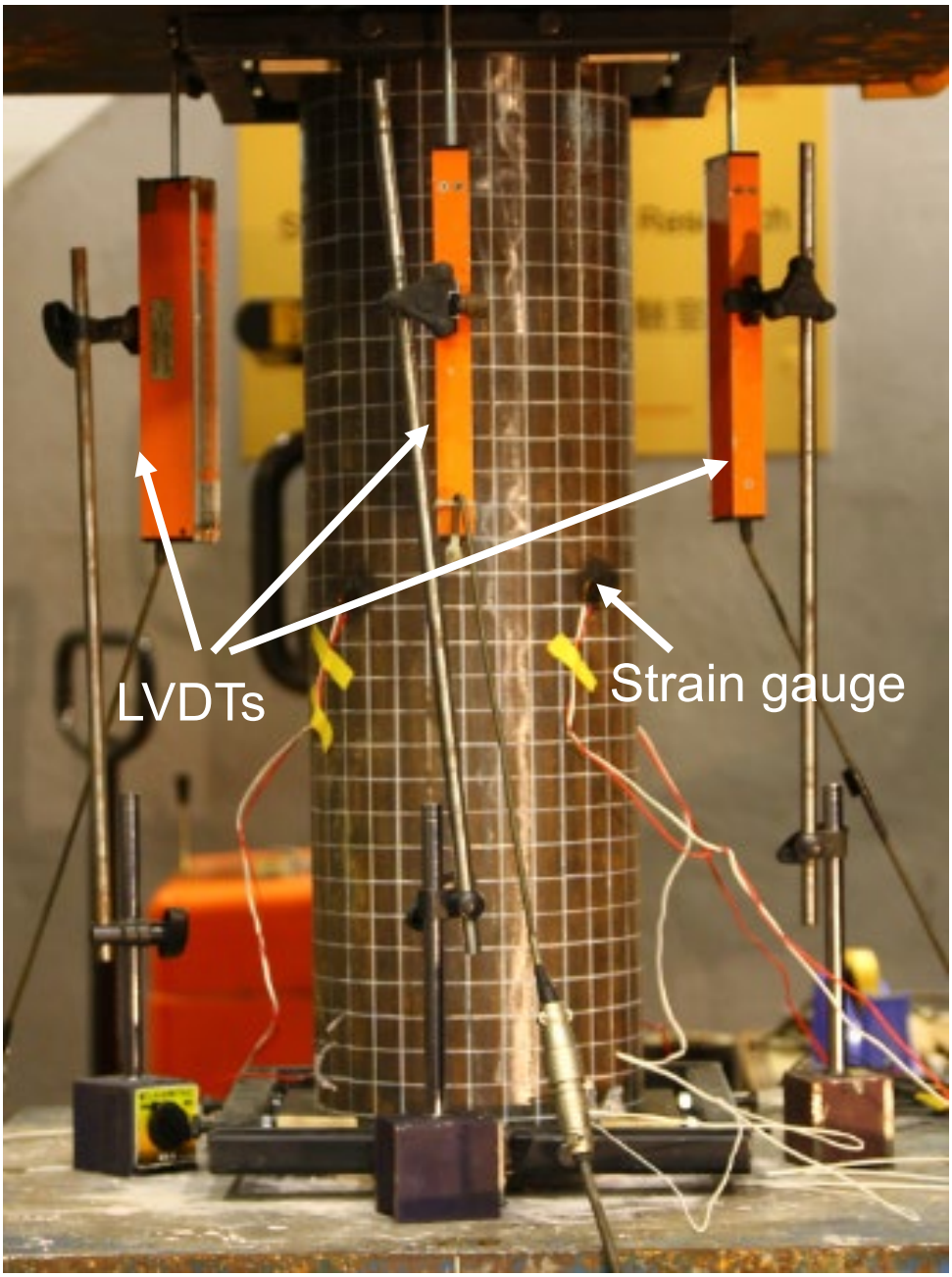

(b) Test set-up

Figure 3. Arrangement of the instrumentations and test set up

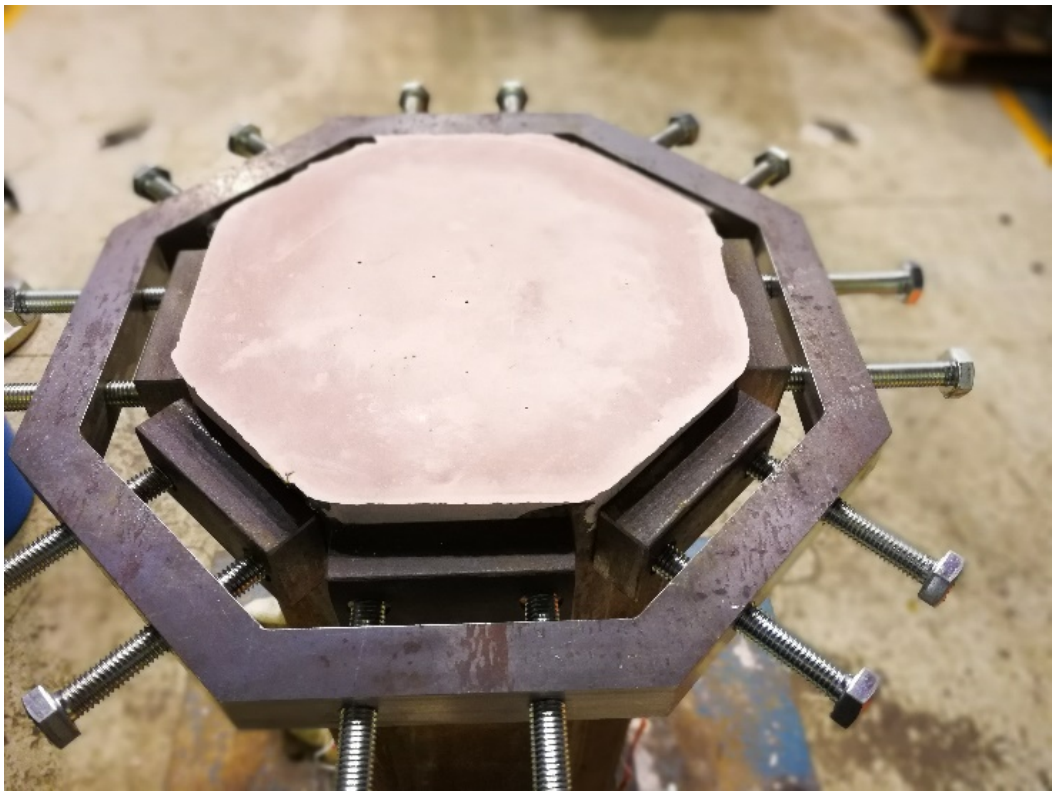

Figure 4. Steel ring at the column end

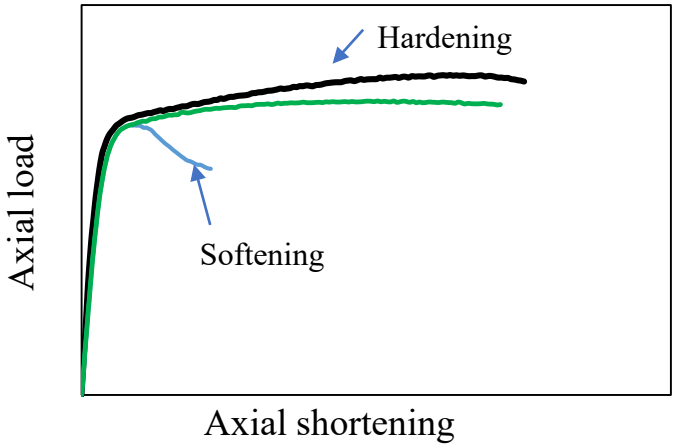

Figure 5. Schematic load-shortening curves for CFST

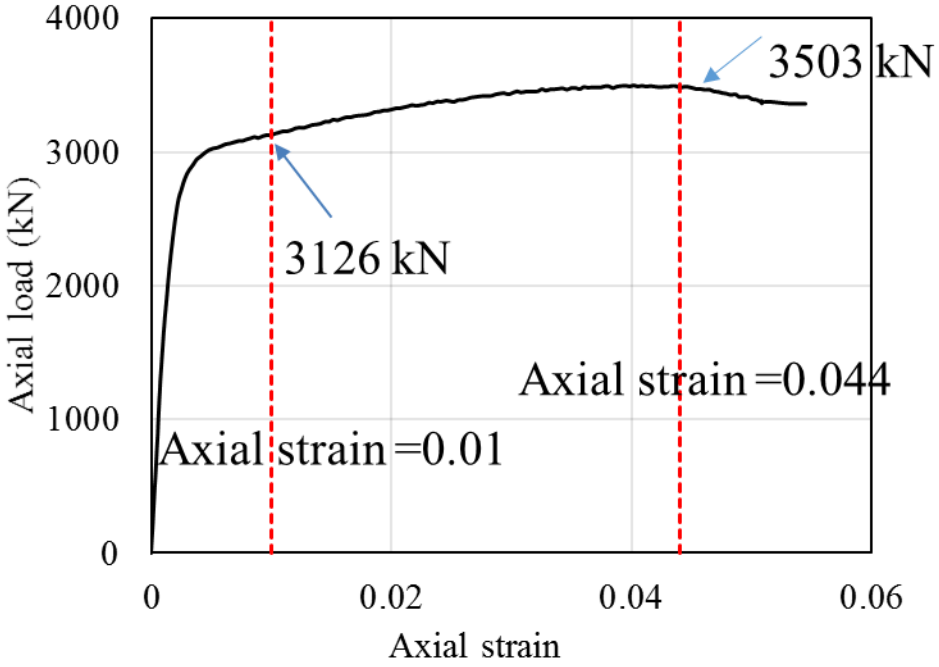

Figure 6. Definition of load capacity (Specimen 30C-1)

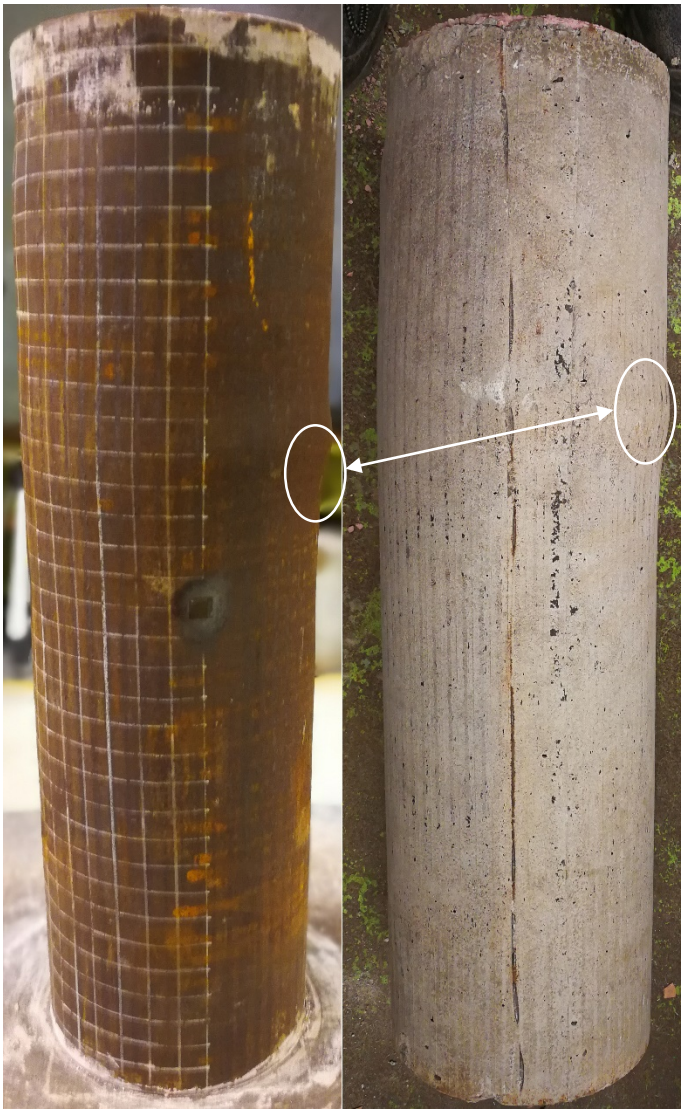

Figure 7. Typical failure mode for CFST (Specimen - 30C-1).

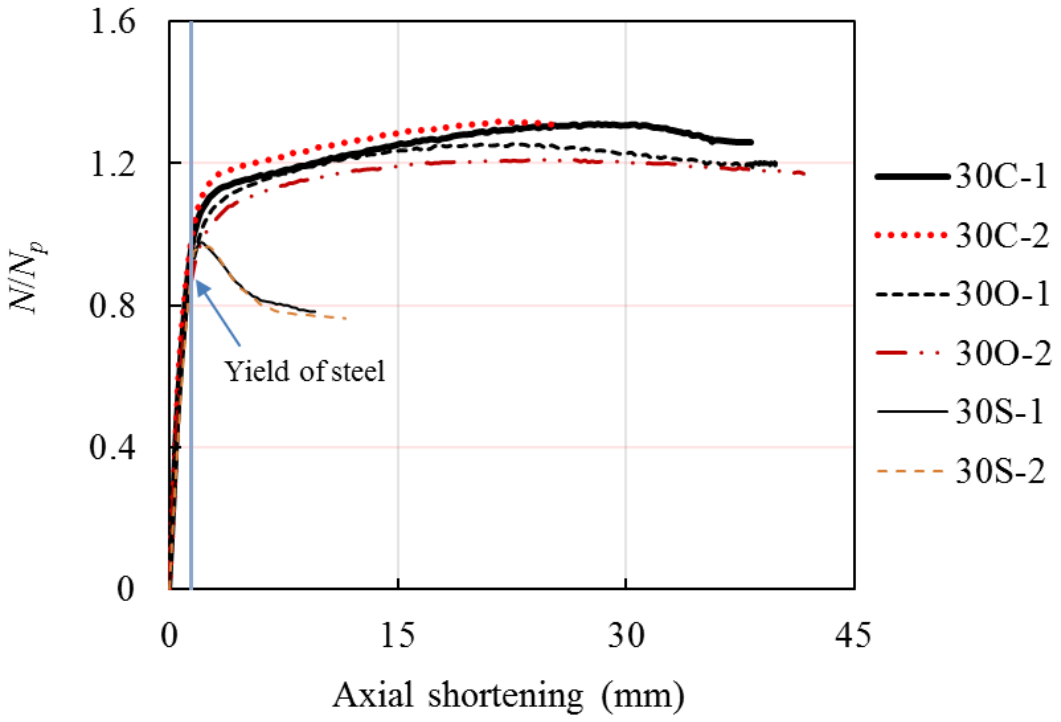

a) C25/30

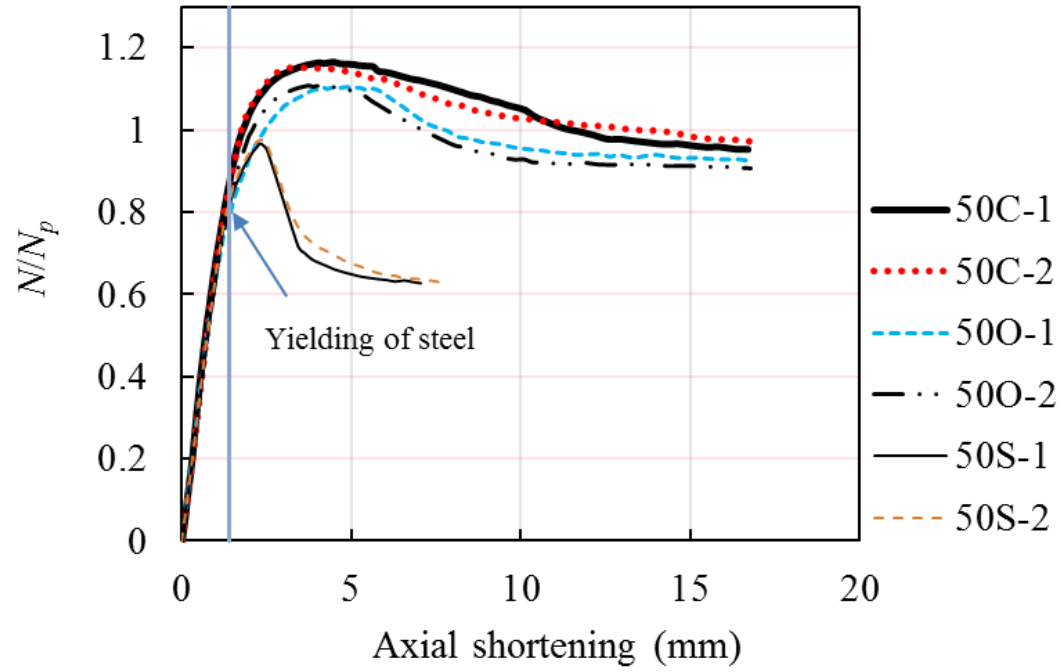

b) C50/60

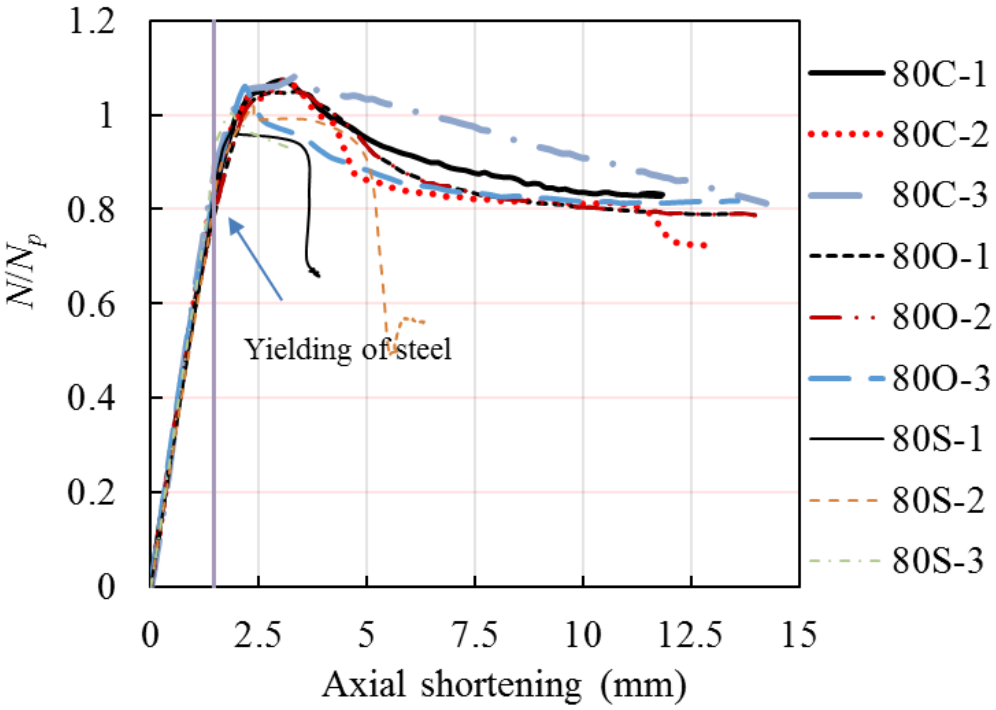

c) C80/95

Figure 8. Load-end shortening curves of test specimens

30C-1

50C-1

50O-1

50S-1

80O-1

Figure 9. Failure mode of typical specimens

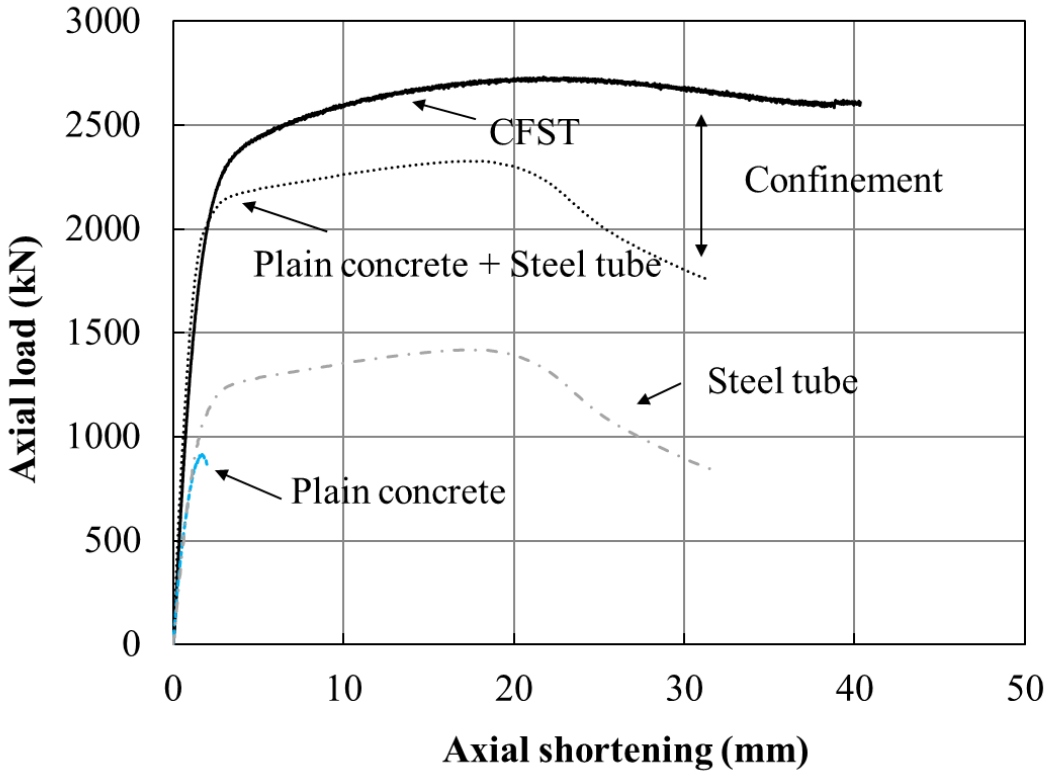

Figure 10. Typical comparison of load-end shortening curves of CFST and a simple superposition model (Specimen: 30O-1)

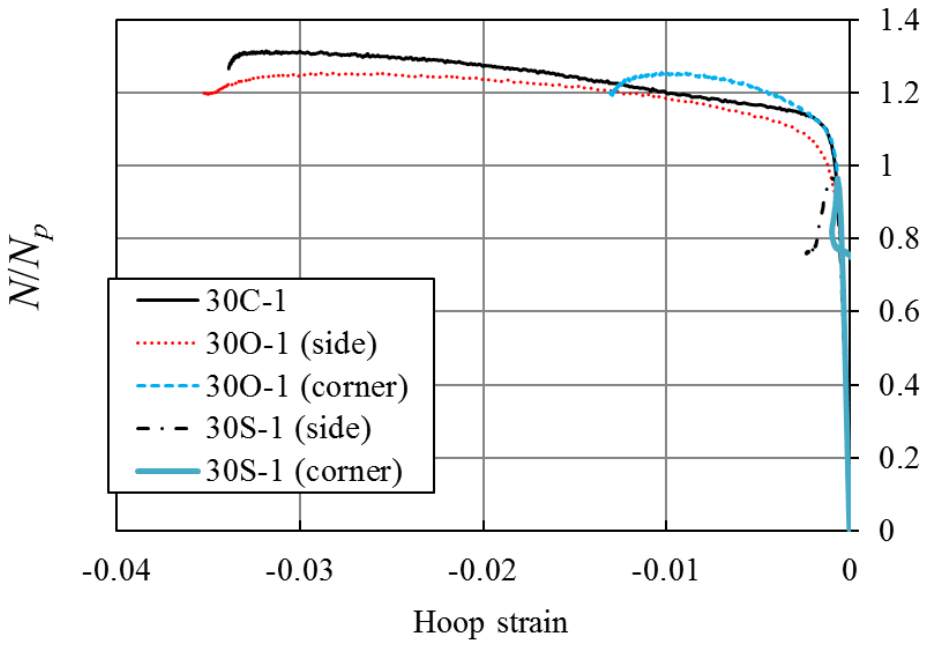

a) C25/30

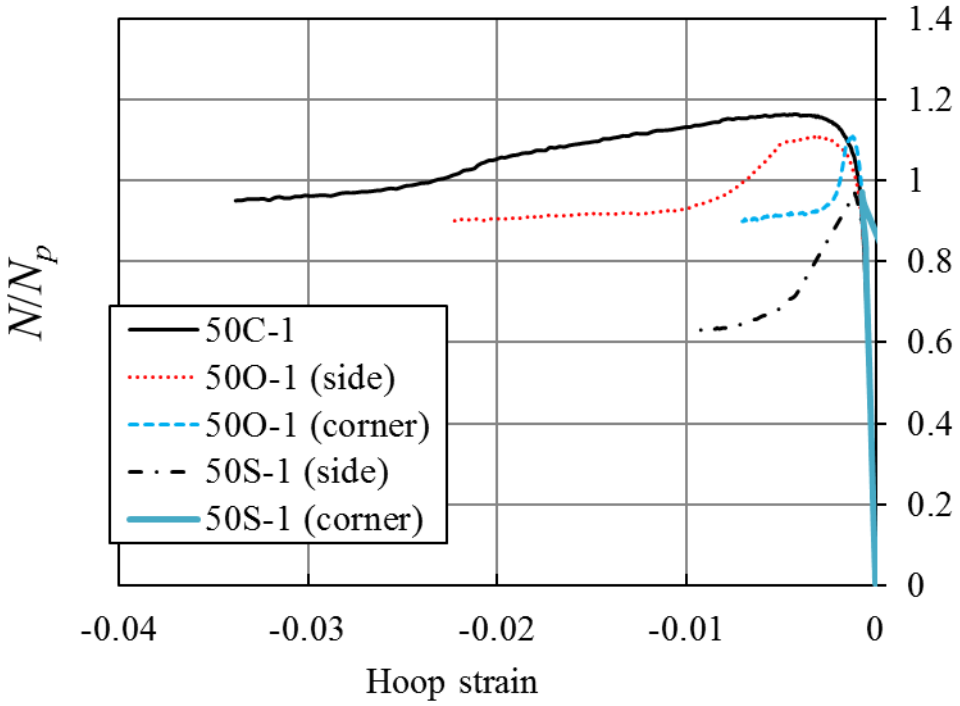

b) C50/60

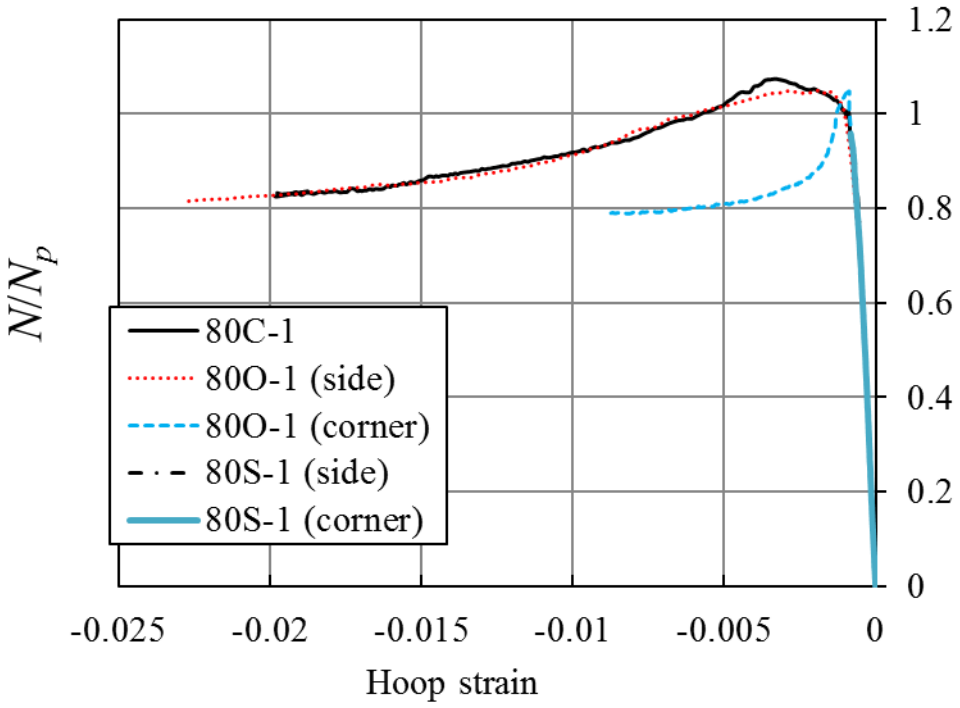

c) C80/95

Figure 11. Load-hoop strain curves of test specimens

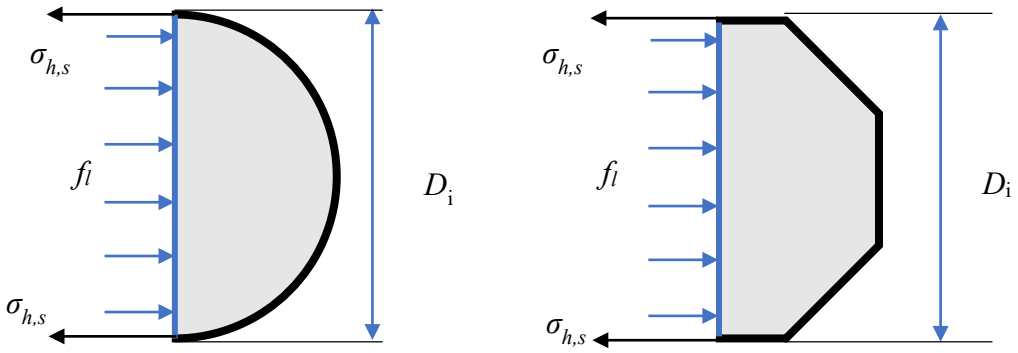

Figure 12. Force-equilibrium condition of circular and octagonal CFST (Liu *et al.* 2017)

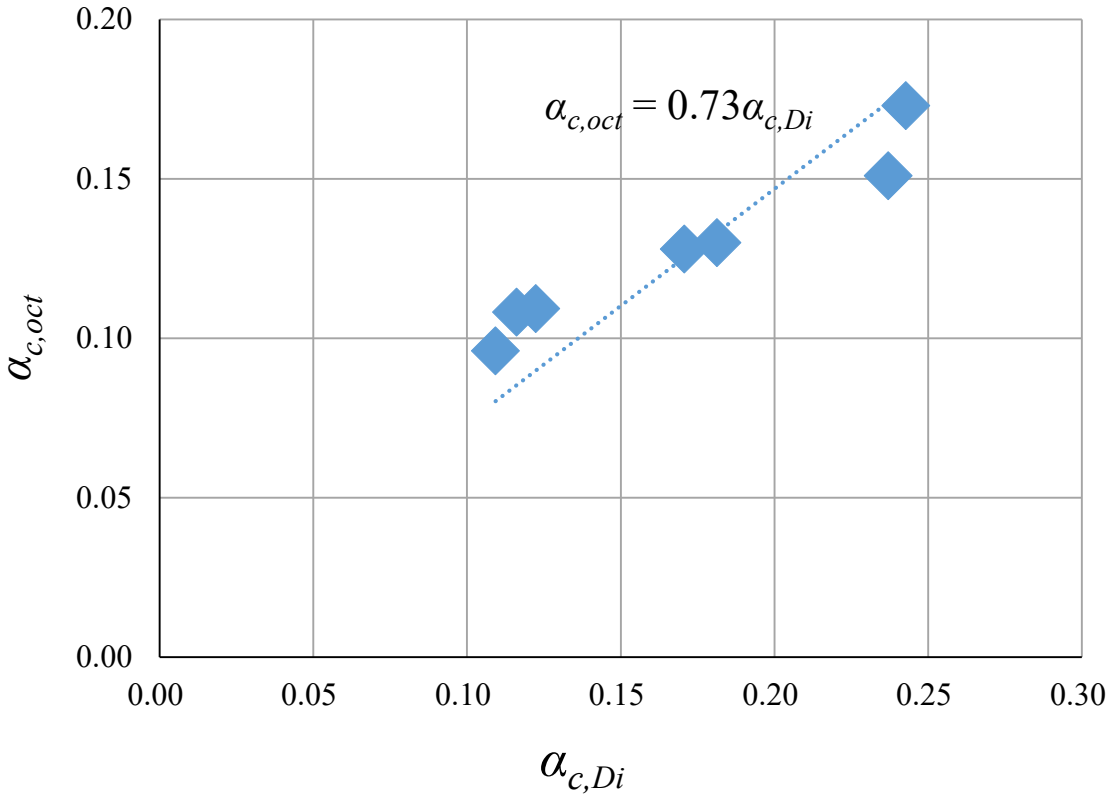

Figure 13. Relationship between the load capacity enhancement percentage in circular and octagonal CFST

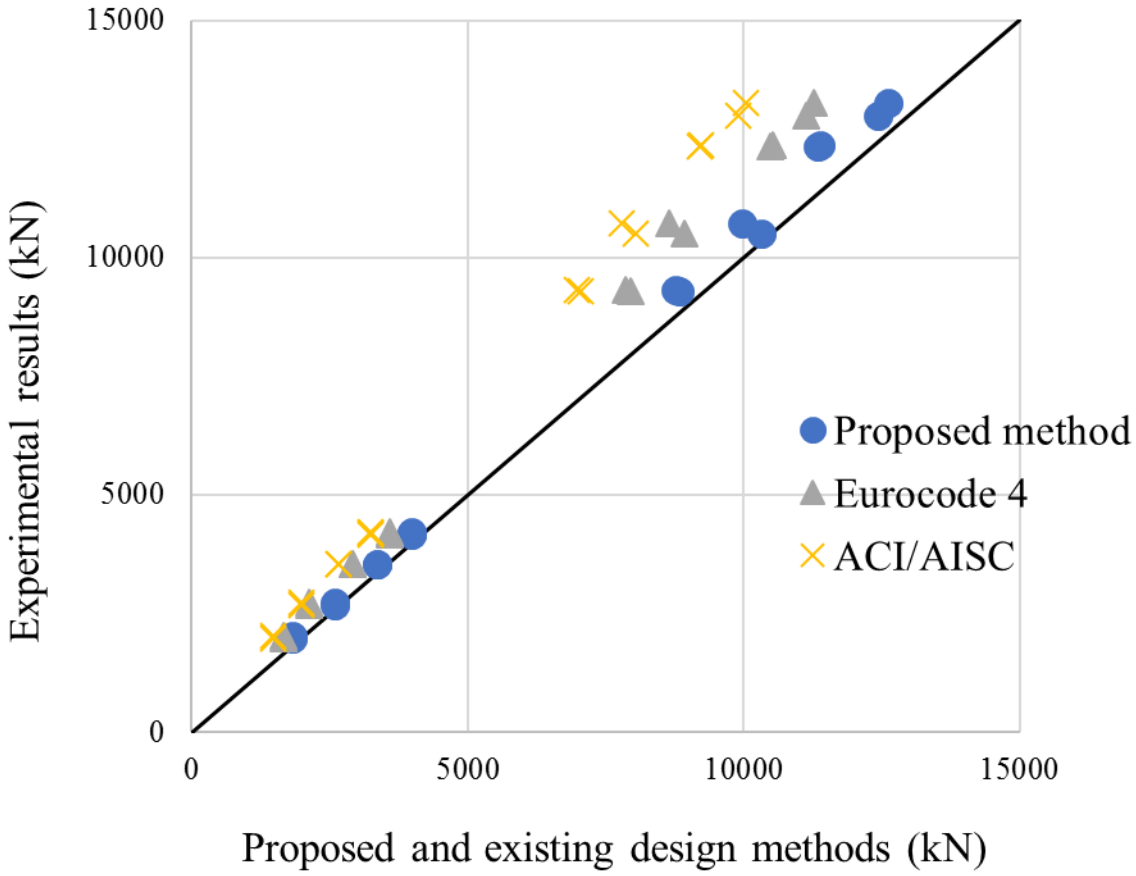

Figure 14. Assessment on the existing and proposed design methods for octagonal CFST